Chern numbers for the two-body Hofstadter-Hubbard butterfly

D. C. Alyuruk and M. Iskin
Department of Physics, Koç University, Rumelifeneri Yolu, 34450 Sarıyer, Istanbul, Türkiye

(Received 14 October 2023; accepted 8 January 2024; published 22 January 2024)

We analyze the two-body spectrum within the Hofstadter-Hubbard model on a square lattice through an exact variational ansatz and study the topological properties of its low-lying two-body bound-state branches. In particular, we discuss how the Hofstadter-Hubbard butterfly of the two-body branches evolves as a function of onsite interactions and how to efficiently calculate their Chern numbers using the Fukui-Hatsugai-Suzuki approach. Our numerical results are fully consistent with the simple picture that appears in the strong-coupling limit, where the attraction between fermions forms a composite boson characterized by an effective hopping parameter and an effective magnetic-flux ratio.

DOI: 10.1103/PhysRevB.109.035149

I. INTRODUCTION

The Hofstadter model has made a profound impact on condensed-matter physics [1,2]. Despite its simplicity, the intricate interplay of Aharonov-Bohm phase and lattice periodicity not only provides crucial insights into the behavior of electrons moving across a solid-state crystal in the presence of an external magnetic field but also shines a spotlight on one of its most intriguing aspects, i.e., the first Chern number. As long as a Bloch band remains isolated in the one-body spectrum, i.e., separated by finite energy gaps from the other bands, its associated Chern number remains constant or "protected" upon alterations in the magnetic field strength or the lattice potential. More importantly, the Chern number C_n of the nth Bloch band determines the contribution of this band to the Hall conductivity [3]. This is in such a way that, when the Fermi energy ε_F lies within an energy gap labeled by j, the Hall conductivity is given precisely by $\sigma_{xy} = \sigma_j e^2/h$, where $\sigma_j = \sum_n C_n$ is a sum over the filled Bloch bands. Since the integer σ_j cannot change continuously, this result reveals that the Hall conductivity is a topological invariant of the system, providing insight into the observed robustness of the integer quantum Hall effect. In a broader context, Chern numbers have become central to our exploration of topological phases of matter, illuminating phenomena as diverse as the quantum Hall effect, topological insulators, topological superconductors, and some other behavior of exotic materials under extreme conditions [4,5]. On the other hand, the Hubbard model is often used for probing the effects of strong electron-electron interactions on material properties, ranging from emergent phenomena such as Mott insulators, high-temperature superconductivity, charge-density waves, and magnetic ordering [6]. It allows us to study how complex and unexpected properties emerge from the collective behavior of strongly-correlated electrons.

To explore how topology influences the behavior of strongly-correlated electrons and vice versa, here we merge the Hofstadter and Hubbard models [7–14]. In particular, we analyze the two-body problem and formulate a two-body Chern number for the low-lying bound-state branches of the Hofstadter-Hubbard model by drawing an analogy with the Fukui-Hatsugai-Suzuki method [15]. It is gratifying to observe that our approach successfully reproduces not only the anticipated butterfly spectrum but also the Chern numbers associated with a strongly bound composite boson in the strong-coupling limit, where the composite boson is characterized by an effective hopping parameter and an effective magnetic-flux ratio. This correspondence arises from the fundamental principle that the topological properties of a two-body branch remain unchanged as long as the energy spectrum remains gapped, which holds true all the way from the infinitely strong-coupling limit down to a finite critical interaction threshold. Below this threshold, a two-body continuum begins to overlap, marking a transition in the system's behavior. We note that there are many recent works on topological aspects of the two-body problem in various multiband lattices [16–26]. They mostly rely on mapping the problem to an effective Hamiltonian for the composite bosons in the strong-coupling limit. In addition there are some past works on the interacting butterflies in the Harper model [27–29]. Our formulation has a minor overlap with the existing literature, and it offers a fresh perspective on this long-standing problem.

The rest of the paper is organized as follows. In Sec. II we introduce the usual Hofstadter model, and its one-body spectrum. In Sec. III we introduce the Hofstadter-Hubbard model, and discuss its two-body spectrum. There we construct the two-body butterflies in Sec. III A, and calculate their Chern numbers in Sec. III B. The paper ends with a brief summary of our conclusions and an outlook in Sec. IV.

II. HOFSTADTER MODEL

Within the tight-binding approximation, the single-particle Hamiltonian for a generic lattice can be written as $\mathcal{H}_\sigma = -\sum_{Si;S'i'} t^\sigma_{Si;S'i'} c^\dagger_{Si\sigma} c_{S'i'\sigma}$, where the hopping parameter $t^\sigma_{Si;S'i'}$ describes tunneling of a spin $\sigma \in \{\uparrow, \downarrow\}$ fermion from the sublattice site S' in the unit cell i' to the sublattice site S in the unit cell i. In this paper we consider a square lattice lying in the xy plane, and set $t^\uparrow_{Si;S'i'} = t^\downarrow_{Si;S'i'} = -t$ for the nearest-neighbor hoppings and 0 otherwise. The presence of an external

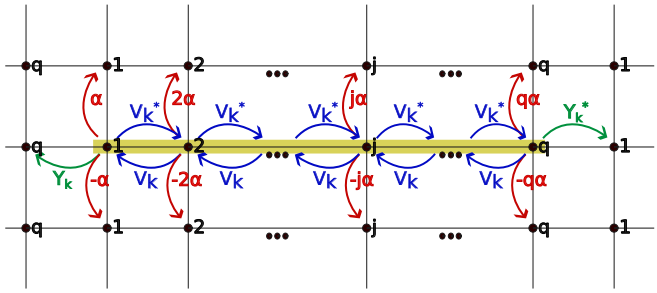

FIG. 1. Magnetic unit cell is highlighted in yellow together with its intraunit cell ($V_{\mathbf{k}}$) and interunit cell ($Y_{\mathbf{k}}$ and $Z^j_{\mathbf{k}}$) hoppings. Sublattice sites are labeled as $S \in \{1, 2, \ldots, j, \ldots q\}$. Here the particle picks up $\pm j\alpha$ phases from upward and downward hoppings, respectively, leading to $Z^j_{\mathbf{k}}$.

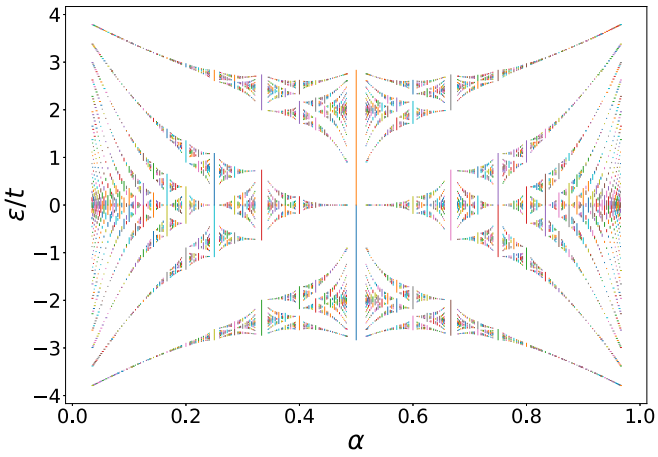

FIG. 2. One-body Hofstadter butterfly for the Bloch bands, where $\alpha = p/q$ is the number of magnetic-flux quantum per cell. Here p and q are relatively prime numbers, and $q_{\max} = 30$ with all possible p/q ratios. Different Bloch bands are shown in different colors for better visibility, where the total bandwidths of the Bloch bands are $8t$ in the $\alpha \to \{0, 1\}$ limits.

magnetic field $\mathbf{B}(\mathbf{r}) = \nabla \times \mathbf{A}(\mathbf{r})$ is taken into account through the Peierls substitution $t \to te^{i2\pi\phi_{Si;S'i'}}$ with $t > 0$, where the phase factor $\phi_{Si;S'i'} = \frac{1}{\varphi_0}\int_{\mathbf{r}_{S'i'}}^{\mathbf{r}_{Si}} \mathbf{A}(\mathbf{r}) \cdot d\mathbf{r}$ takes into account the corresponding vector gauge field [30]. Here φ_0 is the magnetic-flux quantum and $\mathbf{r}_{Si}$ is the position of the site $S \in i$. We are interested in the original Hofstadter model [1], where a uniform magnetic field $\mathbf{B}(\mathbf{r}) = B\hat{\mathbf{z}}$ is perpendicular to a square lattice, and use the Landau gauge $\mathbf{A}(\mathbf{r}) = (0, Bx)$. This is such that the particle accumulates $\sum_{\square} \phi_{Si;S'i'} = Ba^2/\varphi_0 = \alpha$ uniformly after traversing around any one of the cells in the counter-clockwise direction, where a is the lattice spacing and α corresponds to the number of magnetic-flux quanta per cell. We assume $\alpha \equiv p/q$ corresponds precisely to a ratio of two relatively prime numbers p and q. In this case the presence of such a B field leads to a (magnetic) unit cell that has q sites in the x direction, and we label its sublattice sites as $S \in \{1, 2, \ldots, q\}$. The unit cell is illustrated in Fig. 1.

Next we use the canonical transformation $c^\dagger_{Si\sigma} = \frac{1}{\sqrt{N_c}}\sum_{\mathbf{k}} e^{-i\mathbf{k}\cdot\mathbf{r}_i} c^\dagger_{S\mathbf{k}\sigma}$, where N_c is the number of unit cells in the system and $\mathbf{r}_i$ is the position of unit cell i, and express $\mathcal{H}_\sigma$ in the reciprocal space. Here $\mathbf{k} = (k_x, k_y)$ is the crystal momentum (in units of $\hbar \to 1$, the Plack constant) in the first magnetic Brillouin zone (MBZ), where $0 \leqslant k_x < \frac{2\pi}{qa}$ and $0 \leqslant k_y < \frac{2\pi}{a}$ are such that $\sum_{\mathbf{k}} 1 = N_c$. Note that the total number of cells (or equivalently total number of lattice sites) in the system is $N = qN_c$. This leads to the Bloch Hamiltonian for the Hofstadter model $\mathcal{H}_\sigma = \sum_{SS'\mathbf{k}} h^{SS'}_{\mathbf{k}} c^\dagger_{S\mathbf{k}\sigma} c_{S'\mathbf{k}\sigma}$ written in the sublattice basis, where the Hamiltonian matrix

$$\mathbf{h}_{\mathbf{k}} = \begin{pmatrix} Z^1_{\mathbf{k}} & V_{\mathbf{k}} & 0 & . & 0 & Y^*_{\mathbf{k}} \\ V^*_{\mathbf{k}} & Z^2_{\mathbf{k}} & V_{\mathbf{k}} & 0 & . & 0 \\ 0 & \ddots & \ddots & \ddots & 0 & . \\ . & 0 & V^*_{\mathbf{k}} & Z^j_{\mathbf{k}} & V_{\mathbf{k}} & 0 \\ 0 & . & 0 & \ddots & \ddots & \ddots \\ Y_{\mathbf{k}} & 0 & . & 0 & V^*_{\mathbf{k}} & Z^q_{\mathbf{k}} \end{pmatrix} \tag{1}$$

is $q \times q$. Here $Z^j_{\mathbf{k}} = 2t\cos(2\pi j\alpha - k_y a)$ describes interunit cell hoppings in the y direction, and $V_{\mathbf{k}} = t$ and $Y_{\mathbf{k}} = te^{ik_x qa}$ describe, respectively, the intraunit cell and interunit cell hoppings in the x direction with the periodic boundary conditions. These processes are illustrated in Fig. 1. The resultant eigenvalue problem

$$\sum_{S'} h^{SS'}_{\mathbf{k}} n_{S'\mathbf{k}} = \varepsilon_{n\mathbf{k}} n_{S\mathbf{k}} \tag{2}$$

leads to q Bloch bands in the one-body spectrum, which can be labeled as $n \in \{1, 2, \ldots, q\}$, starting with the lowest band. Here $n_{S\mathbf{k}}$ is the projection of the Bloch state onto sublattice S. The spectrum preserves inversion symmetry $\varepsilon_{n\mathbf{k}} = \varepsilon_{n,-\mathbf{k}}$ as a direct manifestation of the gauge invariance in a uniform flux; it has $\varepsilon_{n\mathbf{k}} = -\varepsilon_{q-n,-\mathbf{k}}$ symmetry due to the particle-hole symmetry on a bipartite lattice, and it is mirror symmetric $\varepsilon_{n\mathbf{k}}(\alpha) = \varepsilon_{n\mathbf{k}}(1-\alpha)$ around $\alpha = 1/2$ for $0 \leqslant \alpha \leqslant 1$ [1,31]. When q is an even denominator, these symmetries imply $\varepsilon_{q/2,\mathbf{k}} = -\varepsilon_{q/2+1,\mathbf{k}}$, so that the centrally symmetric $n = q/2$ and $n = q/2 + 1$ bands touch q times with each other at zero energy leading to q Dirac cones in the MBZ. Some of these features are visible in Fig. 2.

Furthermore, one of the elegant aspects of the Hofstadter model is that the competition between the magnetic length scale (i.e., the magnetic cyclotron radius) and the periodicity of the square lattice is known to produce a fractal pattern when bandwidths of the Bloch bands are plotted against α [1,32]. As shown in Fig. 2, since the shape of this pattern looks like the wings of a butterfly, it is usually referred to as the Hofstadter butterfly in the literature. Having introduced the underlying one-body problem, next we analyze the two-body problem.

III. HOFSTADTER-HUBBARD MODEL

Assuming a spin-1/2 system, the Hamiltonian for the Hofstadter-Hubbard model can be written as $\mathcal{H} = \mathcal{H}_0 + \mathcal{H}_{\uparrow\downarrow}$, where $\mathcal{H}_0 = \sum_\sigma \mathcal{H}_\sigma$ is the hopping part, and $\mathcal{H}_{\uparrow\downarrow} = -U\sum_{Si} c^\dagger_{Si\uparrow} c^\dagger_{Si\downarrow} c_{Si\downarrow} c_{Si\uparrow}$ takes the onsite interactions between $\uparrow$ and $\downarrow$ fermions into account with $U \geqslant 0$ the strength of the attraction [33]. Using the canonical transformation given above, and upon transformation $c^\dagger_{n\mathbf{k}\sigma} = \sum_S n_{S\mathbf{k}} c^\dagger_{S\mathbf{k}\sigma}$ to the

band basis, $\mathcal{H}$ can be written as [34]

$$\mathcal{H} = \sum_{n\mathbf{k}} \varepsilon_{n\mathbf{k}} c^\dagger_{n\mathbf{k}\sigma} c_{n\mathbf{k}\sigma} - \frac{U}{N_c} \sum_{\substack{nmn'm' \\ S\mathbf{k}\mathbf{k}'\mathbf{Q}}} n^*_{S\mathbf{k}} m^*_{S,\mathbf{Q}-\mathbf{k}} \times m'_{S,\mathbf{Q}-\mathbf{k}'} n'_{S\mathbf{k}'} c^\dagger_{n\mathbf{k}\uparrow} c^\dagger_{m,\mathbf{Q}-\mathbf{k},\downarrow} c_{m',\mathbf{Q}-\mathbf{k}',\downarrow} c_{n'\mathbf{k}'\uparrow}. \quad (3)$$

We emphasize that this is the exact analog of the Hofstadter-Hubbard model in reciprocal lattice, and it is a convenient starting point for the analysis of the two-body spectrum as it explicitly conserves the center-of-mass momentum $\mathbf{Q}$ of the incoming and outgoing particles.

A. Two-body Hofstadter-Hubbard butterfly

Noting that the onsite interactions allow solely a spin-singlet state, and explicitly conserving the center-of-mass momentum $\mathbf{K}$ of the particles, the two-body spectrum $E_\mathbf{K}$ can be obtained exactly through the following ansatz [35]

$$|\psi_\mathbf{K}\rangle = \sum_{nm\mathbf{k}} \alpha^\mathbf{k}_{nm}(\mathbf{K}) c^\dagger_{n\mathbf{k}\uparrow} c^\dagger_{m,\mathbf{K}-\mathbf{k},\downarrow} |0\rangle, \quad (4)$$

where the variational parameters satisfy $\alpha^\mathbf{k}_{nm}(\mathbf{K}) = \alpha^{\mathbf{K}-\mathbf{k}}_{mn}(\mathbf{K})$, and $|0\rangle$ refers to the vacuum of particles. Through the functional minimization of $\langle\psi_\mathbf{K}|\mathcal{H} - E_\mathbf{K}|\psi_\mathbf{K}\rangle$ with respect to $\alpha^\mathbf{k}_{nm}(\mathbf{K})$, we obtain a set of linear equations given by [35]

$$(\varepsilon_{n\mathbf{k}} + \varepsilon_{m,\mathbf{K}-\mathbf{k}} - E_\mathbf{K})\alpha^\mathbf{k}_{nm}(\mathbf{K}) = \frac{U}{N_c} \sum_{n'm'\mathbf{k}'S} n^*_{S\mathbf{k}} m^*_{S,\mathbf{K}-\mathbf{k}} m'_{S,\mathbf{K}-\mathbf{k}'} n'_{S\mathbf{k}'} \alpha^{\mathbf{k}'}_{n'm'}(\mathbf{K}). \quad (5)$$

Thus, for any given $\mathbf{K}$, $E_\mathbf{K}$ can be determined by recasting Eq. (5) as an eigenvalue problem in the form of a $q^2N_c \times q^2N_c$ matrix. It turns out a typical two-body spectrum has three different sets of solutions [34]. For a given $\mathbf{K}$, there are (i) $q(q+1)/2$ two-body scattering continua, (ii) a number of weakly-bound two-body bound states that always lie in between the scattering continua even in the $U/t \to \infty$ limit, and (iii) q two-body bound states at the bottom of the spectrum which are allowed to become strongly bound in the $U/t \to \infty$ limit. In this paper we are interested in formulating the Chern numbers of the low-lying two-body branches that appear at the bottom of the spectrum with a finite energy gap. As an illustration, we set $K_y = 0$, $\alpha = 1/3$, and $U = 10t$ in Fig. 3, and present the resultant $E_\mathbf{K}$ as a function of K_x. The colored pair of lines are determined by $\max(\varepsilon_{n\mathbf{k}} + \varepsilon_{m,\mathbf{K}-\mathbf{k}})$ and $\min(\varepsilon_{n\mathbf{k}} + \varepsilon_{m,\mathbf{K}-\mathbf{k}})$ for a given (n,m) combination, and six different pairs correspond to upper and lower edges of six possible two-body continua when $q = 3$. In addition, there are three low-lying two-body bound-state branches with energies $E_\mathbf{K} \sim -U$ when $q = 3$.

A more powerful yet efficient way of finding the low-lying two-body branches of interest is as follows. By defining a new set of variational parameters $\beta_{S\mathbf{K}} = \sum_{nm\mathbf{k}} \alpha^\mathbf{k}_{nm}(\mathbf{K}) n_{S\mathbf{k}} m_{S,\mathbf{K}-\mathbf{k}}$, we recast Eq. (5) as a nonlinear-eigenvalue problem [26]

$$\mathbf{G}_\mathbf{K}\boldsymbol{\beta}_\mathbf{K} = 0, \quad (6)$$

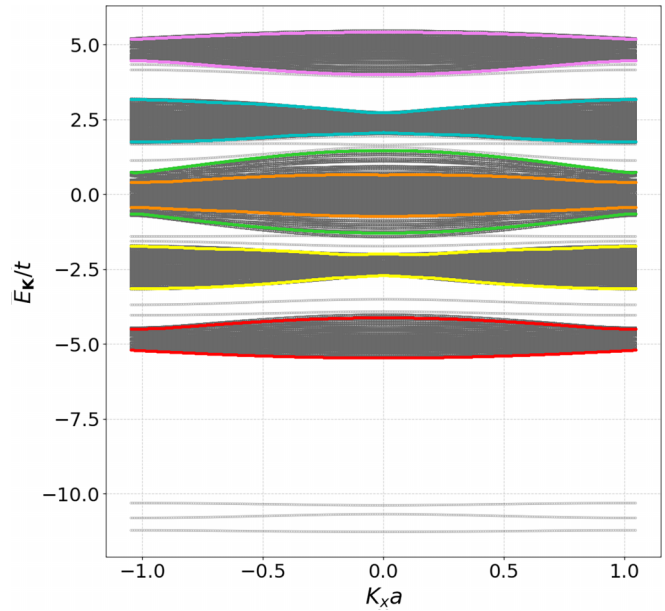

FIG. 3. Full two-body spectrum $E_\mathbf{K}$ as a function of $K_x \in$ MBZ when $K_y = 0$ and $N = 8100$. Gray data corresponds to solutions of Eq. (5) for $\alpha = 1/3$ when $U = 10t$. Six pairs of colored lines are guides to the eye for the six different possible sets of two-body continua discussed in the text. In this paper we are interested in the Chern numbers of the low-lying two-body branches that appear at the bottom of the spectrum.

where $\mathbf{G}_\mathbf{K}$ is a $q \times q$ Hermitian matrix in the sublattice basis with elements

$$G^{SS'}_\mathbf{K} = \delta_{SS'} - \frac{U}{N_c} \sum_{nm\mathbf{k}} \frac{n^*_{S'\mathbf{k}} m^*_{S',\mathbf{K}-\mathbf{k}} m_{S,\mathbf{K}-\mathbf{k}} n_{S\mathbf{k}}}{\varepsilon_{n\mathbf{k}} + \varepsilon_{m,\mathbf{K}-\mathbf{k}} - E_\mathbf{K}}. \quad (7)$$

Then we classify and distinguish solutions of Eq. (6) by setting the eigenvalues of $\mathbf{G}_\mathbf{K}$ to 0 one at a time. For a given $\mathbf{K}$, this is equivalent to q uncoupled nonlinear self-consistency equations for $E_\mathbf{K}$, and we keep only the lowest converging $E_\mathbf{K}$ solution from each equation. This leads to q bound states for a given $\mathbf{K}$, and we label them as $E_{\ell\mathbf{K}}$ where the index $\ell = \{1, 2, \ldots, q\}$ starts with the lowest two-body branch. It turns out a particular two-body branch is associated with a particular eigenvalue of $\mathbf{G}_\mathbf{K}$ for every $\mathbf{K} \in$ MBZ, e.g., setting its third eigenvalue to zero may produce fifth branch. This approach works very well as long as the two-body branch of interest does not overlap with a two-body continuum. As an illustration, we set $\alpha = \{1/3, 1/4, 1/5\}$ and $U = 10t$ in Fig. 4, and present the resultant $E_{\ell\mathbf{K}}$ as a function of $\mathbf{K}$. These results are best understood in the $U/t \to \infty$, where $t_b = 2t^2/U$ and $\alpha_b = 2\alpha \equiv p_b/q_b$ are, respectively, the effective nearest-neighbor hopping parameter and effective number of magnetic-flux quantum per cell for a strongly bound pair of $\uparrow$ and $\downarrow$ particles. Note that, when a bound state breaks up, incurring a cost of binding energy U in the denominator, and its $\uparrow$ constituent hops to a neighboring site, the $\downarrow$ partner follows suit and also hops to the same site. This results in a contribution of t^2 in the numerator, where the prefactor 2 takes into consideration of the possibility of change in the order of spins. Here p_b and q_b are again relatively prime numbers,

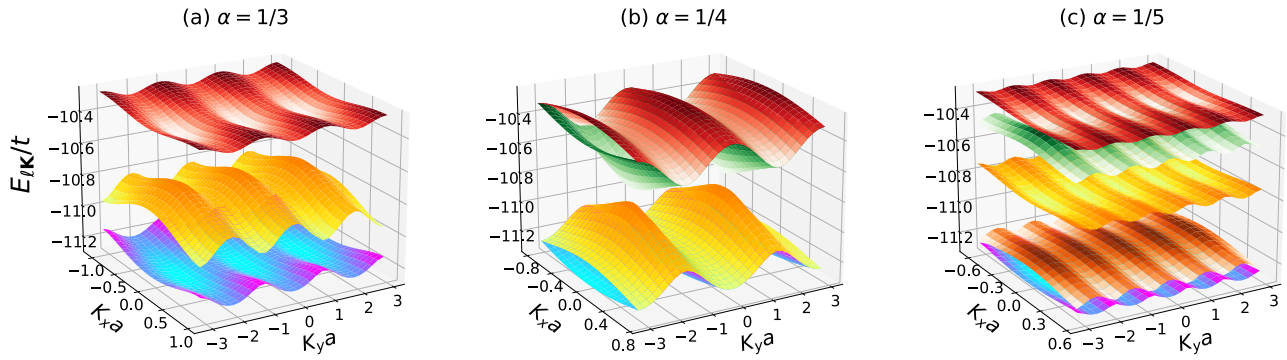

FIG. 4. Low-lying two-body branches $E_{\ell\mathbf{K}}$ as a function of $\mathbf{K} \in$ MBZ, where the index $\ell = \{1, 2, \ldots, q\}$ starts with the lowest-lying branch. These are self-consistent solutions of Eq. (6) for (a) $\alpha = 1/3$, (b) $\alpha = 1/4$, and (c) $\alpha = 1/5$ when $U = 10t$. Note that (a) is identical to the bottom of the spectrum shown in Fig. 3.

i.e., $p_b = p$ and $q_b = q/2$ when q is even. For this reason, Figs. 4(a), 4(b)–4(c) are reminiscent of the effective Bloch bands for a composite boson with $\alpha_b = \{2/3, 1/2, 2/5\}$, below some energy offset (of order $-U$) determined by the binding energy. However, note that since the MBZ of the composite boson is twice the MBZ of its constituent fermions when q is an even denominator, $E_{\ell\mathbf{K}}$ would appear folded when plotted in the MBZ of the fermions. This explains the strange-looking structure of Fig. 4(b).

Enchanted by the intricacies of the one-body Hofstadter butterfly, we construct and present the analogous Hofstadter-Hubbard butterfly for the low-lying two-body branches in Fig. 5, where different two-body branches are shown in different colors for better visibility. For instance, when $U = 10t$, one can extract the bandwidths for the $\alpha_b = \{2/3, 1/2, 2/5\}$ ratios from either Figs. 4 or 5(a). While all of the p/q ratios up to $q_{\max} = 20$ are considered in these butterflies, in cases when different p/q ratios are equivalent to the same p_b/q_b, we show the bandwidths of the Bloch bands for the ratio with the lowest q value. This is why $\alpha_b = 1/3$ has three Bloch bands in Fig. 5 even though it can come from either $\alpha = 2/3$ or $1/6$. In addition, Fig. 4(b) shows that the bandwidths of the nonisolated bands overlap in energy in the even q case, and our coloring scheme does not distinguish these overlapping regions as they can be included in the upper or the lower band. It is pleasing to see that the two-body butterfly shown in Fig. 5(c) bears resemblance to the usual Hofstadter butterfly in the $U/t \gg 1$ limit, where the total bandwidths of the Bloch bands are approximately $8t_b = 16t^2/U$ when $\alpha_b \to \{0^+, 1^-\}$. The two-body butterflies are centered around $-U - 8t^2/U$, because, when a bound state breaks up at a cost of U, one of its constituents can hop to a neighboring site and then come back to the original site to recombine. This leads to an effective onsite energy $2z_{nn}t^2/U$ for the pair, where the prefactor 2 accounts for the possible hopping of the other constituent, and $z_{nn} = 4$ is the number of nearest neighbors on a square lattice [26]. Having discussed the low-lying two-body branches, next we analyze their Chern numbers.

B. Two-body Chern number

As discussed in Sec. III A, the low-lying two-body spectrum $E_{\ell\mathbf{K}}$ can be determined by setting the eigenvalues of $\mathbf{G}_{\mathbf{K}}$ to zero one at a time. Here we show that the associated eigenvectors of Eq. (6), i.e., $\boldsymbol{\beta}_{\ell\mathbf{K}} = (\beta_{1\ell\mathbf{K}}, \beta_{2\ell\mathbf{K}}, \ldots, \beta_{q\ell\mathbf{K}})^{\mathrm{T}}$ in the sublattice basis with T the transpose, can be used to characterize the topology of the low-lying two-body branches [26,36]. For this purpose, we follow closely the Fukui-Hatsugai-Suzuki approach that is developed for the usual Hofstadter model [15], and define the so-called link variable as

$$\mathcal{U}^{\boldsymbol{\mu}}_{\ell\mathbf{K}_j} = \frac{\sum_S \beta^*_{S\ell\mathbf{K}_j}\beta_{S\ell,\mathbf{K}_j+\hat{\boldsymbol{\mu}}}}{\left|\sum_S \beta^*_{S\ell\mathbf{K}_j}\beta_{S\ell,\mathbf{K}_j+\hat{\boldsymbol{\mu}}}\right|} \tag{8}$$

for the ℓth branch, where $\mathbf{K}_j = (\frac{2\pi}{q_b N_x a} j_x, \frac{2\pi}{N_y a} j_y)$ with $j_x = \{0, 1, 2, \ldots, N_x - 1\}$, and $j_y = \{0, 1, 2, \ldots, N_y - 1\}$ denotes the position of a lattice point in the effective MBZ. Furthermore, $\hat{\boldsymbol{\mu}} \in \{\hat{\mathbf{x}}, \hat{\mathbf{y}}\}$ is a vector pointing along the K_x or K_y axis in the effective MBZ, where $\hat{\mathbf{x}} = (\frac{2\pi}{q_b N_x a}, 0)$ and $\hat{\mathbf{y}} = (0, \frac{2\pi}{N_y a})$. Note that $N_c = N_x N_y$ is the number of primitive unit cells, and we choose $q_b N_x = N_y$. In addition, the eigenvectors $\boldsymbol{\beta}_{\ell\mathbf{K}}$ are periodic in the reciprocal space by construction, where $\beta_{S\ell\mathbf{K}_j} = \beta_{S\ell,\mathbf{K}_j+N_x\hat{\mathbf{x}}} = \beta_{S\ell,\mathbf{K}_j+N_y\hat{\mathbf{y}}}$. Then we define the so-called field strength by

$$F_{\ell\mathbf{K}_j} = \ln\left[\mathcal{U}^{\mathbf{x}}_{\ell\mathbf{K}_j}\mathcal{U}^{\mathbf{y}}_{\ell,\mathbf{K}_j+\hat{\mathbf{x}}}\left(\mathcal{U}^{\mathbf{x}}_{\ell,\mathbf{K}_j+\hat{\mathbf{y}}}\right)^{-1}\left(\mathcal{U}^{\mathbf{y}}_{\ell\mathbf{K}_j}\right)^{-1}\right] \tag{9}$$

for the ℓth branch, within the principal branch of the logarithm where $-\pi < \frac{1}{\mathrm{i}}F_{\ell\mathbf{K}_j} \leqslant \pi$ counts the accumulated phase after traversing the cell around the point $\mathbf{K}_j$ (which corresponds to the left-lower corner of the cell) in the counter-clockwise direction. This leads to the Chern number of the ℓth low-lying two-body branch as [15]

$$C_\ell = \frac{1}{2\pi\mathrm{i}}\sum_{j_x j_y} F_{\ell\mathbf{K}_j}, \tag{10}$$

where the summation covers the effective MBZ. Note that C_ℓ can only be defined when the ℓth branch is well separated from other states, i.e., when it satisfies the gap-opening condition $|E_{\ell\mathbf{K}} - E_{\ell\pm1,\mathbf{K}}| \neq 0$ for all $\mathbf{K} \in$ MBZ states in the sufficiently large U/t regime.

Our approach works very well and reproduces the anticipated C_ℓ above a critical U threshold (which is approximately of the order of the total bandwidth W_α of the Bloch bands for a given α) as long as the two-body branch of interest does not overlap with another two-body branch or a two-

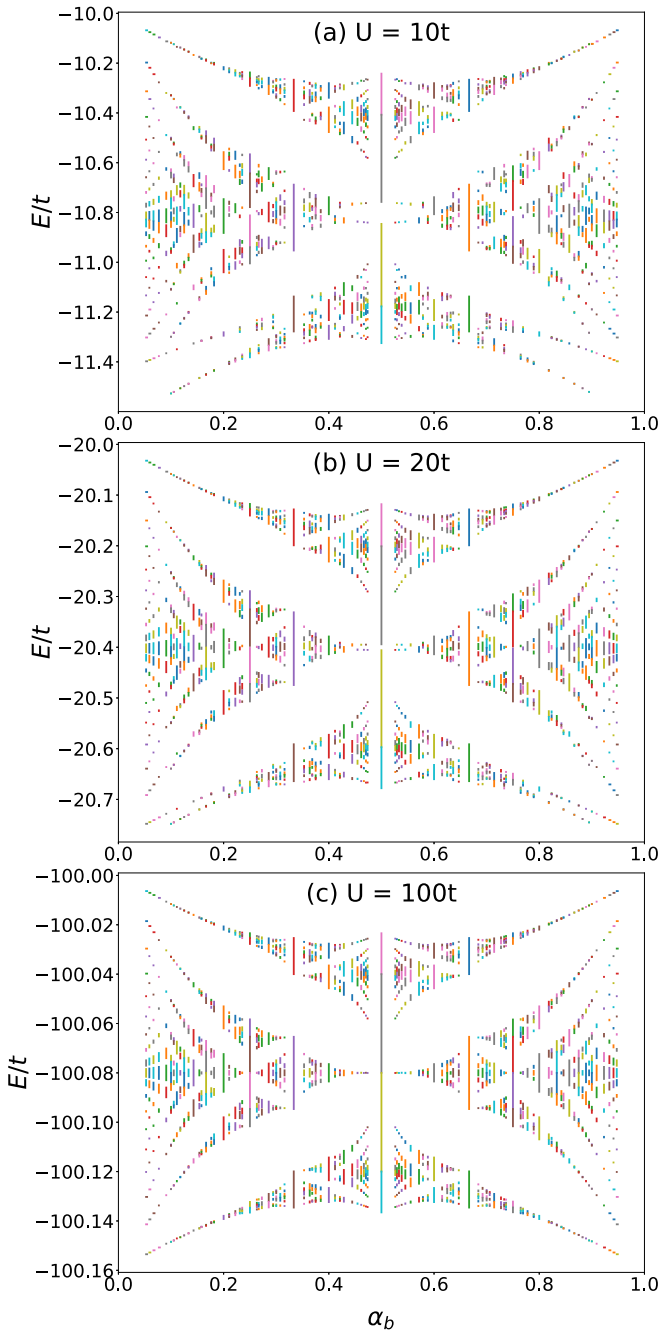

FIG. 5. Two-body Hofstadter-Hubbard butterfly for the low-lying two-body branches, where $\alpha_b \equiv p_b/q_b$ is the effective number of magnetic-flux quantum per cell for the bound states. Here p_b and q_b are relatively prime numbers where $q_{\max} = 20$ with all possible p/q ratios. Interaction strength U/t is set to 10 in (a), 20 in (b), and 100 in (c). Different two-body branches are shown in different colors for better visibility, where their total bandwidths scale as $8t_b = 16t^2/U$ in the $\alpha_b \to \{0, 1\}$ limits, and they are centered around $-U - 8t^2/U$.

body continuum. For instance, when $\alpha = p/q$ in the usual Hofstadter model, the Chern number of the jth energy gap in the Bloch spectrum is known to satisfy the Diophantine equation $\sigma_j \equiv sj$ in mod q, where s is the modular inverse of p, i.e., $sp \equiv 1$ in mod q [3,37]. Thus, $\sigma_j = \sum_{n \leqslant j} C_n$, where C_n is the Chern number of the nth Bloch band with the index $n = \{1, 2, \ldots, q\}$ starting from the lowest-lying one. The Diophantine equation leaves a mod q ambiguity in σ_j, except for the 0th and qth gap in which case $\sigma_0 = \sigma_q = 0$ corresponds, respectively, to a trivial particle vacuum and a trivial band insulator. This ambiguity was resolved for the Hofstadter model on the rectangular lattice [3,37], leading to the constraint $\sigma_j \in [1 - \frac{q}{2}, \frac{q}{2} - 1]$ when q is an even denominator, and to the constraint $\sigma_j \in [-\frac{q-1}{2}, \frac{q-1}{2}]$ when q is an odd denominator. For example, since $s = 1$ when $\alpha = 1/3$, we find $\sigma_j = \{0, 1, 2, 0\}$ from the Diophantine equation, leading to $\sigma_j \to \{0, 1, -1, 0\}$ for the jth gap in the constraining interval and to $C_n \to \{+1, -2, +1\}$ for the Bloch bands. Similarly, since $s = 2$ when $\alpha = 2/3$, we find $\sigma_j = \{0, 2, 1, 0\}$ from the Diophantine equation, leading to $\sigma_j \to \{0, -1, +1, 0\}$ in the constraining interval, and to $C_n \to \{-1, +2, -1\}$ for the Bloch bands. Similarly, since $s = 3$ when $\alpha = 2/5$, we find $\sigma_j = \{0, 3, 1, 4, 2, 0\}$ from the Diophantine equation, leading to $\sigma_j \to \{0, -2, +1, -1, +2, 0\}$ in the constraining interval and to $C_n \to \{-2, +3, -2, +3, -2\}$ for the Bloch bands. These are in perfect agreement with our numerical C_ℓ values, where the effective flux ratios are $\alpha_b = \{1/3, 2/3, 2/5\}$ for the bound states when $\alpha = \{2/3, 1/3, 1/5\}$. We also checked many other flux ratios, e.g., $C_\ell = \{-3, +4, -3, +4, -3, +4, -3\}$ when $\alpha = 1/7$, and $C_\ell = \{-1, -1, 2, 2, -1, -1\}$ when $\alpha_\uparrow = 1/2$ is different from $\alpha_\downarrow = 1/3$ [38]. Note that the middle branches $\ell = \{3, 4\}$ are not energetically isolated and touch each other in the latter case since $\alpha_b = \alpha_\uparrow + \alpha_\downarrow = 5/6$ has an even denominator, i.e., C_3 and C_4 are not well defined.

IV. CONCLUSION

In summary, here we analyzed the two-body problem within the Hofstadter-Hubbard model, with a particular focus on its low-lying two-body bound-state branches. In particular we studied evolution of their two-body Hofstadter-Hubbard butterfly as a function of the interaction strength U, and formulated their Chern numbers C_ℓ in an efficient way by making an analogy with the Fukui-Hatsugai-Suzuki method [15]. Our numerical results at finite U are in perfect agreement with the expected Chern numbers associated with a composite boson in the $U/t \to \infty$ limit, where $t_b = 2t^2/U$ and $\alpha_b = 2\alpha$ are, respectively, the effective hopping parameter and effective magnetic-flux ratio. This is because the topological nature of a two-body branch cannot change as long as its spectrum remains gapped, which turns out to be the case down to a critical threshold $U \sim W_\alpha$ determined by the total bandwidth W_α of the Bloch bands for a given α, below which the low-lying two-body branches start overlapping with a two-body continuum.

Recent studies have highlighted the significance of the Chern number of a Bloch band within topological band theory [4], where it serves as a powerful tool for characterizing and comprehending the topological characteristics of electronic band structures in various materials. For instance it plays a pivotal role in classifying topological phases, elucidating the quantization of the Hall conductance, and predicting the emergence of novel electronic states [5]. Similarly, the Chern number of a two-body bound-state branch may find some potential applications and utility in certain physical phenom-

ena, and its fate will be determined in time. It is worth emphasizing that our formalism is quite generic and valid not only for attractive ($U > 0$) and repulsive ($U < 0$) onsite interactions, but also it is readily applicable to all sorts of lattice geometries. As an outlook we expect the single-particle bulk-boundary correspondence to apply to the two-body topological phase as well. For instance, similar to the recent results on the interacting Haldane model [19,26], one can verify that the two-body Chern numbers of the interacting Hofstadter model are also in agreement with the chirality of the edge states through an exact diagonalization with open boundary conditions [39]. In addition we expect the two-body analog of the conventional Hall conductance to be $\bar{\sigma}_{xy} = \bar{\sigma}_j \frac{\bar{e}^2}{h}$, where $\bar{\sigma}_j = \sum_\ell C_\ell$ and $\bar{e} = 2e$ is the effective charge of the pairs. Finally, it is possible to extend our approach to finite-range interactions, which is underway.

ACKNOWLEDGMENT

The authors acknowledge funding from TÜBİTAK.

[1] D. R. Hofstadter, Energy levels and wave functions of bloch electrons in rational and irrational magnetic fields, Phys. Rev. B **14**, 2239 (1976).

[2] I. I. Satija, *The Butterfly in the Quantum World: The Story of the Most Fascinating Quantum Fractal* (Morgan & Claypool Publishers, 2016).

[3] D. J. Thouless, M. Kohmoto, M. P. Nightingale, and M. den Nijs, Quantized Hall conductance in a two-dimensional periodic potential, Phys. Rev. Lett. **49**, 405 (1982).

[4] A. Bansil, H. Lin, and T. Das, Colloquium: Topological band theory, Rev. Mod. Phys. **88**, 021004 (2016).

[5] S. Rachel, Interacting topological insulators: a review, Rep. Prog. Phys. **81**, 116501 (2018).

[6] D. P. Arovas, E. Berg, S. A. Kivelson, and S. Raghu, The Hubbard model, Annu. Rev. Condens. Matter Phys. **13**, 239 (2022).

[7] H. Zhai, R. O. Umucalılar, and M. O. Oktel, Pairing and vortex lattices for interacting fermions in optical lattices with a large magnetic field, Phys. Rev. Lett. **104**, 145301 (2010).

[8] D. Cocks, P. P. Orth, S. Rachel, M. Buchhold, K. Le Hur, and W. Hofstetter, Time-reversal-invariant Hofstadter-Hubbard model with ultracold fermions, Phys. Rev. Lett. **109**, 205303 (2012).

[9] C. Repellin, T. Yefsah, and A. Sterdyniak, Creating a bosonic fractional quantum Hall state by pairing fermions, Phys. Rev. B **96**, 161111(R) (2017).

[10] R. O. Umucalılar and M. Iskin, BCS theory of time-reversal-symmetric Hofstadter-Hubbard model, Phys. Rev. Lett. **119**, 085301 (2017).

[11] C. Zeng, T. D. Stanescu, C. Zhang, V. W. Scarola, and S. Tewari, Majorana corner modes with solitons in an attractive Hubbard-Hofstadter model of cold atom optical lattices, Phys. Rev. Lett. **123**, 060402 (2019).

[12] D. Shaffer, J. Wang, and L. H. Santos, Theory of Hofstadter superconductors, Phys. Rev. B **104**, 184501 (2021).

[13] B. Andrews, T. Neupert, and G. Möller, Stability, phase transitions, and numerical breakdown of fractional chern insulators in higher Chern bands of the Hofstadter model, Phys. Rev. B **104**, 125107 (2021).

[14] D. Shaffer, J. Wang, and L. H. Santos, Unconventional self-similar Hofstadter superconductivity from repulsive interactions, Nat. Commun. **13**, 7785 (2022).

[15] T. Fukui, Y. Hatsugai, and H. Suzuki, Chern numbers in discretized Brillouin zone: efficient method of computing (spin) Hall conductances, J. Phys. Soc. Jpn. **74**, 1674 (2005).

[16] H. Guo and S.-Q. Shen, Topological phase in a one-dimensional interacting fermion system, Phys. Rev. B **84**, 195107 (2011).

[17] M. A. Gorlach and A. N. Poddubny, Topological edge states of bound photon pairs, Phys. Rev. A **95**, 053866 (2017).

[18] A. Marques and R. Dias, Topological bound states in interacting Su–Schrieffer–Heeger rings, J. Phys.: Condens. Matter **30**, 305601 (2018).

[19] G. Salerno, M. Di Liberto, C. Menotti, and I. Carusotto, Topological two-body bound states in the interacting Haldane model, Phys. Rev. A **97**, 013637 (2018).

[20] L. Lin, Y. Ke, and C. Lee, Interaction-induced topological bound states and Thouless pumping in a one-dimensional optical lattice, Phys. Rev. A **101**, 023620 (2020).

[21] J. Zurita, C. E. Creffield, and G. Platero, Topology and interactions in the photonic Creutz and Creutz-Hubbard ladders, Adv. Quantum Technol. **3**, 1900105 (2020).

[22] G. Salerno, G. Palumbo, N. Goldman, and M. Di Liberto, Interaction-induced lattices for bound states: Designing flat bands, quantized pumps, and higher-order topological insulators for doublons, Phys. Rev. Res. **2**, 013348 (2020).

[23] G. Pelegrí, A. M. Marques, V. Ahufinger, J. Mompart, and R. G. Dias, Interaction-induced topological properties of two bosons in flat-band systems, Phys. Rev. Res. **2**, 033267 (2020).

[24] Z.-W. Zuo, W. A. Benalcazar, Y. Liu, and C.-X. Liu, Topological phases of the dimerized Hofstadter butterfly, J. Phys. D **54**, 414004 (2021).

[25] N. Okuma and T. Mizoguchi, Relationship between two-particle topology and fractional Chern insulator, Phys. Rev. Res. **5**, 013112 (2023).

[26] M. Iskin, Topological two-body bands in a multiband Hubbard model, Phys. Rev. A **107**, 053323 (2023).

[27] A. Barelli, J. Bellissard, P. Jacquod, and D. L. Shepelyansky, Double butterfly spectrum for two interacting particles in the Harper model, Phys. Rev. Lett. **77**, 4752 (1996).

[28] A. Barelli, J. Bellissard, P. Jacquod, and D. L. Shepelyansky, Two interacting Hofstadter butterflies, Phys. Rev. B **55**, 9524 (1997).

[29] H. Doh and S.-H. S. Salk, Effects of electron correlations on the Hofstadter spectrum, Phys. Rev. B **57**, 1312 (1998).

[30] Since the Zeeman coupling to the spin does not have any effect on the two-body problem (see Ref. [38]), it is not considered in this paper.

[31] The mirror symmetry around $\alpha = 1/2$ can be deduced from the following observations: (i) changing the direction of the magnetic field, i.e., $\alpha \to -\alpha$, cannot have any effect on the

spectrum, and (ii) Eq. (1) is invariant under the addition of $2\pi j$ to the argument of cosine in $Z_{\mathbf{k}}^{-j}$.

[32] B. Andrews, HofstadterTools: A python package for analyzing the Hofstadter model, arXiv:2311.18726 [cond-mat.mes-hall].

[33] Our formalism is valid for both attractive ($U > 0$) and repulsive ($U < 0$) interactions. For instance, in the latter case, Eq. (6) can be used to determine the high-lying two-body branches which appear at the top of the two-body spectrum. They are also known as the repulsively bound doublon states in the literature [40]. Note that such states do not appear in free-space models because, unlike the lattice models that feature a finite bandwidth, the parabolic one-body spectrum is not bounded from above.

[34] M. Iskin and A. Keleş, Stability of $(N+1)$-body fermion clusters in a multiband Hubbard model, Phys. Rev. A **106**, 033304 (2022).

[35] M. Iskin, Two-body problem in a multiband lattice and the role of quantum geometry, Phys. Rev. A **103**, 053311 (2021).

[36] See Ref. [26] for an alternative formulation of the two-body Chern number that is in association with a two-body Berry curvature. However, that formulation is not exact by construction, it produces accurate results only in the $U/t \gg 1$ limit, and it converges very slowly to the expected integers in the $N_c \to \infty$ limit. Furthermore, our current formulation is very efficient, and it yields correct integers above a critical N_c threshold, which is typically very small depending on q and U/t.

[37] J. Avron, O. Kenneth, and G. Yehoshua, A study of the ambiguity in the solutions to the Diophantine equation for Chern numbers, J. Phys. A: Math. Theor. **47**, 185202 (2014).

[38] We note that, in the general case when the $\uparrow$ and $\downarrow$ fermions have distinct one-body spectra, i.e., when $\mathbf{h}_{\mathbf{k}}^{\uparrow} \neq \mathbf{h}_{\mathbf{k}}^{\downarrow}$, one needs to replace the Bloch bands $\varepsilon_{n\mathbf{k}} \to \varepsilon_{n\mathbf{k}\uparrow}$ and $\varepsilon_{m,\mathbf{K}-\mathbf{k}} \to \varepsilon_{m,\mathbf{K}-\mathbf{k},\downarrow}$ and the Bloch factors $n_{S\mathbf{k}} \to n_{S\mathbf{k}\uparrow}$ and $m_{S,\mathbf{K}-\mathbf{k}} \to m_{S,\mathbf{K}-\mathbf{k},\downarrow}$ accordingly in Eqs. (5) and (7) [35].

[39] Y. Hatsugai, Chern number and edge states in the integer quantum Hall effect, Phys. Rev. Lett. **71**, 3697 (1993).

[40] K. Winkler, G. Thalhammer, F. Lang, R. Grimm, J. Hecker Denschlag, A. Daley, A. Kantian, H. Büchler, and P. Zoller, Repulsively bound atom pairs in an optical lattice, Nature (London) **441**, 853 (2006).